NJC

Accepted Manuscript

This is an *Accepted Manuscript*, which has been through the Royal Society of Chemistry peer review process and has been accepted for publication.

Accepted Manuscripts are published online shortly after acceptance, before technical editing, formatting and proof reading. Using this free service, authors can make their results available to the community, in citable form, before we publish the edited article. We will replace this *Accepted Manuscript* with the edited and formatted *Advance Article* as soon as it is available.

You can find more information about *Accepted Manuscripts* in the Information for Authors.

Please note that technical editing may introduce minor changes to the text and/or graphics, which may alter content. The journal's standard Terms & Conditions and the Ethical guidelines still apply. In no event shall the Royal Society of Chemistry be held responsible for any errors or omissions in this *Accepted Manuscript* or any consequences arising from the use of any information it contains.

ROYAL SOCIETY OF CHEMISTRY

www.rsc.org/njc

Application of the energetic span model to the electrochemical catalysis of proton reduction by a diiron azadithiolate complex

Marc Bourrez, Frederic Gloaguen

UMR 6521, CNRS, Université de Bretagne Occidentale, Brest, France

E-mail: marc.bourrez@univ-brest.fr (MB); fgloague@univ-brest.fr (FG)

Abstract

Computational methods, such as DFT calculations, have emerged as a powerful tool to study the homogeneous catalysis of electrochemical reactions involved in renewable fuel production. Here, we report an adaptation of the energetic span model to obtain, from DFT calculations, key metrics of the catalysis of electrochemical H_2 production by the diiron azadithiolate complex [Fe_2(μ-SCH_2NHCH_2S)$(CO)_6$] (**1**). The main advantage of our approach is that both thermodynamic and kinetic effects on the turnover frequency (TOF) can be computed in a simple way. By taking into account the influence of the electrode potential on TOF determining intermediates (TDI) and TOF determining transition states (TDTS), we calculated a TOF vs. overpotential relationship that shows three different kinetic regimes. This finding is consistent with the catalytic mechanism derived from the analysis of voltammetric responses of **1** in the presence of tosic acid.

Introduction

By definition, a catalyst accelerates the reaction rate by lowering the activation energy $\Delta G^{\neq}$ at a given driving force ΔG.[1,2] In the processes of fuel production from renewable energy sources,[3,4] however, reactions are electrochemical: e.g. proton and carbon dioxide reduction[5–12] or water oxidation.[13–16] In that case, ΔG is proportional to the overpotential $\eta = E - E^0$, where E is the potential at which

catalysis proceeds and E^0 the reversible potential vs. the same reference.[17–19] Thus, a catalyst, that can be the electrode material itself, a grafted molecule or a free-diffusing molecule, increases the rate of the electrochemical reaction for a given overpotential, and therefore the energy efficiency. As the electrochemical reactions that produce fuels involve several steps, a good understanding of the mechanisms is moreover required to guide the design of catalysts that efficiently activate the overall process without requirement of a large overpotential.[20–23]

Numerous transition metal complexes based on Co,[24–28] Ni,[29–32] Fe[33–41] or other transition metals[42–46] have been reported as homogeneous molecular catalysts for the electrochemical reduction of a proton source to hydrogen. Cyclic voltammetry (CV) is usually employed to establish the potential at which catalysis does occur, to measure the catalytic current and to help probe the catalytic mechanism. However, obtaining key metrics of the catalytic activity, such as overpotential and apparent catalytic rate constant, imply a rigorous analysis of the CV responses under varied experimental conditions. To this aim, the group of Costentin, Robert and Savéant has developed a methodology allowing to establish a Tafel's-like relationship between TOF and overpotential, and thus the intrinsic activity of the catalyst at zero overpotential (i.e. TOF_0).[22,23] As a result, molecular catalysts for H_2 production can be benchmarked in a rational way.[47] Computational chemistry methods have been developed in parallel to help analyze experimental data and decipher catalytic cycle. In particular, density functional theory (DFT) calculations have proved useful for establishing the structures of intermediates and transition states and for determining their thermodynamic properties, such as acidity constant and standard electrochemical potential.[20,21,48,49] Recently, few computational studies coupled with microkinetic analysis have dealt with calculation of TOF for the catalysis of electrochemical reactions.[50,51] But, none of these computational studies have lead to establish a Tafel's-like relationship, and a method to do so remains to be developed.

In an attempt to rationalize the effect of the structure of an in-situ generated molecular catalyst on the efficiency of a catalytic cycle, Amatore and Jutand have introduced the concept of energetic span, which is the difference between the top and the bottom of the energy landscape of

the cycle; the smaller the energy span the higher the TOF of the cycle.[1,52] Starting from this concept, Kozuch and coworkers have developed a mathematical model, which allows calculating the TOF from the difference in energy between the most stable intermediate(s) and the least stable transition state(s). It further leads to consider TOF determining intermediates (TDI) and TOF determining transition states (TDTS) instead of a rate-determining step.[52–54] This model has been successfully applied to many different catalytic systems,[55] but has yet to be adapted to the homogeneous catalysis of electrochemical reactions.

Capitalizing on our recent mechanistic study of the catalysis of electrochemical proton reduction by the diiron azadithiolate derivative $[Fe_2(\mu\text{-}SCH_2N(H)CH_2S)(CO)_6]$ (**1**, Scheme 1),[56] we thought to employ DFT to compute the reaction free energies and activation barriers of the catalytic cycle, and then to apply the energetic span model to calculate the TOF of this catalyst as a function of the electrode potential. The calculated value of TOF was then compared to that experimentally determined from analysis of the voltammetric responses in the presence of a moderately strong acid, i.e. tosic acid (HOTs, $pK_a \sim 8.7$ in MeCN).

Materials and methods

Materials

$[Fe_2(\mu\text{-}SCH_2N(H)CH_2S)(CO)_6]$ (**1**) was synthesized according to previously published procedures.[57] All the solutions were prepared from analytical-grade chemicals and HPLC-grade acetonitile (MeCN). Cyclic voltammetry (CV) experiments were carried out in N_2-purged 0.1 M Bu_4NPF_6/MeCN as previously described.[56] All potentials are referred against that of the ferrocenium/ferrocene (Fc^+/Fc) couple used as an internal standard.

Computational method

General procedure. Density functional theory (DFT) calculations were carried out using the ORCA software package.[58] Geometry of the structures was optimized in the gas phase using the B3LYP functional in combination with the def2-TZVP basis set for all atoms. A corresponding effective core potential (ECP) was applied to the Fe atoms.[59] Vibrational analysis and single point energy calculation were performed from the gas phase optimized geometry using same functional and basis set, taking into account effect of the solvent (i.e. MeCN, ε = 36.3) using the conductor-like screening model (COSMO).[60] Calculations were accelerated using the so-called resolution of identity and chain of sphere approximations (RIJCOSX) in conjunction with the def2-TZVP/J auxiliary basis set.[61] Tight convergence criteria were used. For ground states, vibrational analysis showed no imaginary components, while it showed one imaginary component for transition states. Reversible potentials of the electrochemical reactions and pK_a values were calculated using well-established thermodynamic cycles and corrected according to recently published procedures. This approach proved to give accurate results for various types of molecular catalyst.[11,56]

*Procedure for optimization of transition states **TS1***. A relaxed potential energy surface (PES) scan for the rotation of a CO group face-to-face with the NH group was performed from the steady-state intermediate **3** to the *rotated* state. Then a transition state optimization (optTS in Orca terminology) from the structure of highest energy in the preceding PES scan was performed, along with full hessian calculation. Vibrational analysis then showed one imaginary component.

*Procedure for optimization of transition states **TS2***. First, the potential energy surface shown in Figure 2 was constructed. To this aim, several relaxed PES scans were performed, in which the (N)–H_a–H_b–(Fe) distance was incrementally decreased, for constrained Fe–Fe distances from 2.8 to 3.1 Å. For each relaxed PES scan, a transition state optimization was performed first keeping the Fe–Fe distance at its constrained value, and then without any geometric constraints for the lowest-energy transition states found. Vibrational analysis showed one imaginary component.

Procedure for computation of Mayer bond orders (Figure 3). A relaxed PES scan was performed, in which the (N)–H_a–H_b–(Fe) distance was incrementally decreased in **6** until the release

of H_2. From the structures obtained from the PES scan, a single point calculation at the HF/STO-3G level was performed. The values of Mayer bond order were extracted from these single point calculations.[62]

Procedure for calculation of TOF and X_{TOF}. The TOF were calculated using the source code of the Fortran program written by Kozuch *et al*. and compiled with g95 (www.g95.org).[63] The energy diagram was established taking into account the energy difference in both the chemical and electrochemical steps (Table 1). The procedure for calculation of activation energies for the electrochemical steps is detailed in supporting information. The activation energy for protonation steps was set at a value of 4 kcal mol^{-1}, which we believe is a reasonable value for the fast protonation of the amine group ($pK_a \sim 8.2$) in the azadithiolate bridge by a relatively strong acid in MeCN.[64] Furthermore, we found that changing this activation energy between 2 and 6 kcal mol^{-1} had little influence on the computed values TOF or X_{TOF}. In order to compute the TOF at zero-overpotential, which means at virtually zero driving force and therefore TOF $\rightarrow$ 0, the driving force was arbitrarily set at a value of -2 kcal mol^{-1}. This lead to a computed value of TOF at zero-overpotential equal to that obtained by extrapolation of the computed Tafel plot at low overpotential, validating the procedure.

Results and discussion

*Proposed mechanism for the catalysis of proton reduction by **1***

From analysis of voltammetric responses and DFT calculations, we previously proposed that the reduction of moderately strong acid ($pK_a < 10$ in MeCN) mediated by **1** follows the catalytic cycle depicted in Scheme 1.[56] The initial step is the formation at $E_{red,1}$ of the *N*-protonated reduced intermediate **3** (Scheme 2) through a CE process, in which the protonation step C is fast. Then, a tautomerization reaction occurs leading to a putative hydride **4**. A second *N*-protonation gives the

proton-hydride intermediate **5**, which is reduced at a potential close to that of the *N*-protonated intermediate **2** (i.e. $E_{red,2} \sim E_{red,1}$) releasing H_2 and regenerating **1**.

To confirm the proposed catalytic mechanism, we recorded CVs of **1** in the presence of HOTs at low temperature (Figure 1), which is anticipated to slow down the chemical steps occurring in the course of catalysis. At a temperature of −10 °C (263 K), in the absence of a proton source, **1** undergoes a chemically reversible reduction at $E_{1/2}$ = −1.60 V, a potential similar to that measured at room temperature. Addition of 1 to 2 molar equivalent of HOTs triggers the appearance of a chemically irreversible reduction peak at a cathodic peak potential $E_{p,c}$ = −1.32 V (i.e. $E_{red,1}$ in Scheme 1), ascribed to the reduction of the *N*-protonated form **2** (scheme 2). The reduction of **2** is thus negatively shifted by ca. 50 mV when the temperature is decreased from room temperature to −10 °C. A shift of the reduction peak towards more negative potentials is expected when the chemical reaction following the electron transfer is slowed down. However, even at −10° C, the reduction of **2** is chemically irreversible. From these observations, we can conclude that the reduction of **2**, which initially leads to the *N*-protonated and reduced intermediate **3**, is coupled with a fast chemical reaction on the CV timescale. Considering that the reduction of diiron dithiolate complexes strongly increases the basicity of the metal centers,[48,49,56,65,66] it is likely that **3** undergoes a tautomerization reaction leading to the iron-hydride **4**. This assumption is supported by DFT calculations. Addition of HOTs up to 4 molar equivalents triggers the appearance of a new chemically irreversible reduction peak at $E_{p,,c}$ = −1.45 V (i.e. $E_{red,2}$ in Scheme 1). The pK_a of the amine group in **4** was calculated by DFT to be 9.5 in MeCN, which means that the *N*-protonation of **4** by HOTs is thermodynamically downhill (ΔG = −1.2 kcal mol^{-1}). Thus in the presence of an excess of HOTs, the *N*-protonation of **4** gives **5**, which is reduced at a potential slightly more negative than **2**. According to DFT calculations, the reduction of **5** occurs at a potential about 60 mV more negative than that of the reduction of **2.** Upon addition of 12 molar equiv. of HOTs in solution, a catalytic peak with a current enhancement ratio (with i_{cat} the intensity of the peak in the presence of HOTs and $i_{p,0}$ the intensity of the peak with no acid added) $i_{cat}/i_{p,0}$ = 5.2 is observed at $E_{p,c}$ = −1.56V, whereas the peak corresponding to the

reduction of **2** does not increase. Consequently, the reduction of **5** at a potential slightly more negative than that of the reduction of **2** leads to the $\{2H^+/2e^-\}$ intermediate **6**, which eventually releases H_2 regenerating **1**. These observations are fully consistent with the catalytic mechanism depicted in Scheme 1, considering that peak potentials are measured on the CVs, whereas reversible potentials are calculated by DFT.

Computational study of the chemical steps in the course of catalysis

Here, we first calculated the relative free energies of the transition states **TS1** and **TS2** of the chemical steps **3** $\rightarrow$ **4** and **6** $\rightarrow$ **1** + H_2 (Scheme 1). It allowed the estimation of the corresponding rate constant *k*, by applying the Eyring's relationship with the pre-exponential factor set a value $\kappa = 1$.[67] The value of $\Delta G^{\neq}$(**TS1**) is 1.2 kcal mol^{-1}, which indicates that the tautomerization reaction from the reduced N-protonated species **3** to the hydride **4** is almost barrierless and proceeds with a high rate constant of about $k = 8 \times 10^{11}$ s^{-1}. The transition state **TS2** corresponds to the formation of the H–H bond from the $\{2H^+/2e^-\}$ intermediate **6**, the release of H_2 having been found barrierless. The value of $\Delta G^{\neq}$(**TS2**) is 5.5 kcal mol^{-1} corresponding to a rate constant of $k = 7 \times 10^8$ s^{-1}. Analysis of Mayer bond orders[62] in the course of the reaction **6** $\rightarrow$ **1** + H_2 shows that the transition state corresponds to the breaking of the N–H bond concomitantly with the formation of a transient σ-bonded dihydrogen-iron complex (Figure 3). Then, as H_2 is released, **1** relaxes from the rotated state to its ground state.

Energetic landscape as a function of applied potential

In computational study of electrochemical reaction, the effect of the applied potential *E* on the driving force ΔG for electron transfer has to be accounted for. Here, we used the method described by Nørskov and coworkers, which consists in shifting the relative energy of the intermediate after an electron transfer by an amount of $E - E^0$, where E^0 is the reversible potential of the electrochemical step.[68] A reversible potentials for the electron transfer steps **2** $\rightarrow$ **3** and **5** $\rightarrow$ **6** are $E^0 = -1.21$ and

−1.27 V, respectively.[56] The whole reaction profile for the catalysis of the reduction of HOTs by **1** could be computed for a range of different values of applied potential *E* (Figure 4 and Table 1).

In homogeneous catalysis of electrochemical reduction of a proton source HA in non-aqueous solvent, the overpotential η is defined as the difference between the potential *E* at which catalysis proceeds and the reversible potential E^0_{HA}.[17–19] The latter can be calculated from the equation $E^0_{HA} = E^0_{H+/H2} - 0.059 \times pK_{a,HA}$, where $pK_{a,HA}$ is the acidity constant and $E^0_{H+/H2}$ the reversible potential of the solvated proton/hydrogen couple in the same solvent. From tabulated values, we estimate that the reversible potential for the reduction of HOTs in MeCN is E^0_{HA} = −0.54 V. This means that no catalysis of proton reduction can occur at E > −0.54 V when using HOTs as a proton source in MeCN. At potentials between −0.54 V and −1.20 V ($0 < \eta \leq 0.66$ V), where **2** is not fully reduced, the driving force is so weak that all the proton-coupled electron transfer steps of the catalysis are uphill and the overall catalysis is rate-limited by the transfer of two electrons. It should be noted that by using the term "proton coupled electron transfer" no assumption is made on the concerted or stepwise character of the reaction.[69,70] At potentials more negative than that of the reduction **5** ($E < -1.27$ V, $\eta < -0.73$ V), the driving force is so large that all the proton-coupled electron transfer steps of the catalysis are downhill and the overall rate of the catalysis is only limited by the release of H_2 from **6**. Between these two limits, the reduction of **2** is downhill while the reduction of **5** is uphill, consequently the overall catalysis is rate-limited by a proton-coupled electron transfer step.

TOF as a function of applied potential

The procedure developed by Kozuch and coworkers allows for calculating TOF (in s^{-1} for 1 M of catalyst and 1 M of substrate) from the relative energies of intermediates and transition states of the catalytic cycle (Equation (1)), where ΔG_{Ti} is the relative energy of the transition state *i* and ΔG_{Ij} is the relative energy of the intermediate *j*.[53,54]

$$\mathrm{TOF} = \frac{k_B T}{h} \frac{\exp\left(-\Delta G / k_B T\right) - 1}{\sum_{i,j}^{N} \exp\left(\frac{1}{k_B T}\left(\Delta G_{Ti} - \Delta G_{Ij} - \delta G'_{ij}\right)\right)} ; \; \delta G'_{ij} = \Delta G \text{ for } i > j \text{ and } \delta G'_{ij} = 0 \text{ for } i \leq j$$

(1)

Importantly, the energy differences calculated in the denominator of Equation (1) do not only take into account the energy differences between one transition state and one intermediate, but rather every energy differences between each intermediates and each transition states. This consequently leads to consider *rate-determining states* (TDI and TDTS) instead of *rate-determining steps*. From Equation (1), it can easily be seen that the relative energy of some states will have more influence than others on the overall TOF. The degree of TOF control translates the influence of a change in energy of a given state, whether it is an intermediate ($X_{\mathrm{TOF,I}}$) or a transition state ($X_{\mathrm{TOF,TS}}$), on the overall TOF (Equation (2)). A degree of TOF control close to one means that a little change in energy influences the overall TOF.[53,54]

$$X_{\mathrm{TOF,I}} = \left| \frac{1}{\mathrm{TOF}} \frac{\partial \mathrm{TOF}}{\partial \Delta G_{Ij}} \right| \quad \text{and} \quad X_{\mathrm{TOF,TS}} = \left| \frac{1}{\mathrm{TOF}} \frac{\partial \mathrm{TOF}}{\partial \Delta G_{Ti}} \right| \qquad (2)$$

The theoretical TOF of **1** for the catalysis of the reduction of HOTs as a function of the overpotential $\eta = E - E^0_{\mathrm{HA}}$ was calculated from Equation (1) using the Fortran code written by Kozuch *et al*[63] and the energetic landscapes established for a range of value of overpotential (Figure 4 and Table 1). This allowed us to establish a Tafel plot entirely calculated by DFT (Figure 5). Three main kinetic regimes can be observed. At low overpotentials, the slope of the Tafel plot is $2.3 \times RT/2F$ = 30 mV dec^{-1}. This value is indicative of a kinetic regime controlled by the first proton coupled electron transfer steps **1** $\rightarrow$ **3**.[71] This result is confirmed by the analysis of the degree of TOF control of the intermediates showing that the TDIs are **1** and **2**, i.e. the species considered prior to any electron transfer, the TDTS being always **TS2** (Figure 5). At moderate overpotentials (i.e. $-0.5 < \eta < -0.7$V), the slope is $2.3 \times RT/F$ = 59 mV dec $^{-1}$, consistent with a kinetic regime controlled by the second proton coupled electron transfer steps **4** $\rightarrow$ **6**. In this Tafel region, the TDIs are **4** and **5**, i.e. the species considered after the first electron transfer. At high overpotential, the TOF reaches a plateau value of about 10^8 s^{-1},

indicating that the TOF is independent of the applied potential *E* but controlled by the rate of formation and release of H_2. We previously measured the experimental value of the absolute maximum TOF (i.e. the TOF at high overpotential) for the catalysis of the electrochemical reduction of HOTs at ambient temperature, log(TOF, s^{-1}) = (3.0 ± 0.5) for 0.5 mM of **1** and 12 molar equivalent of HOTs.[56] An experimental value of TOF at high overpotential of about 10^8 s^{-1} could be extrapolated for [HOTs] = 1 M of and [**1**] = 1 M, confirming a rough agreement between experimental and computed data at limiting conditions.

Conclusion

We report here a computational method for determining the activity of a homogeneous catalyst for electrochemical proton reduction. This method accounts in a simple way for both thermodynamic and kinetic effects thanks to the energetic span model applied here to an electrocatalytic process. We believe that a similar strategy may be used to establish structure vs. function relationships of other molecular catalysts for electrochemical proton reduction, but also for carbon dioxide reduction and water oxidation. This might become a powerful tool for the rational design of catalysts by computer.[20,21,50,51] We are planning to improve the method described here to take into account bimolecular reactions and concerted proton-coupled electron transfer, which are reaction of primary importance in the reactivity of metal-hydride catalysts.[70,72]

Associated content

Detailed procedure for the calculation of free enthalpies of activation for electrochemical steps and coordinates for **TS1** and **TS2** are given in supporting information.

Acknowledgements

This work was supported by the Agence Nationale de la Recherche (ANR, BLANC SIMI9/0926-1, "TechBioPhyp"), the Centre National de la Recherche Scientifique (CNRS), and the Université de Bretagne Occidentale (UBO).

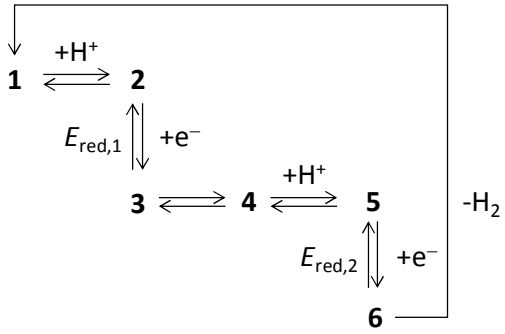

Scheme 1. Proposed mechanism for the catalysis of electrochemical proton reduction by **1** in the presence of relatively strong acid (pK_a < 10 in MeCN). DFT calculations gives: $E_{red,1}$ = −1.21 V, E_{red2} = −1.27 V, pK_a(2/1) = 8.2, pK_a(5/4) = 9.5.

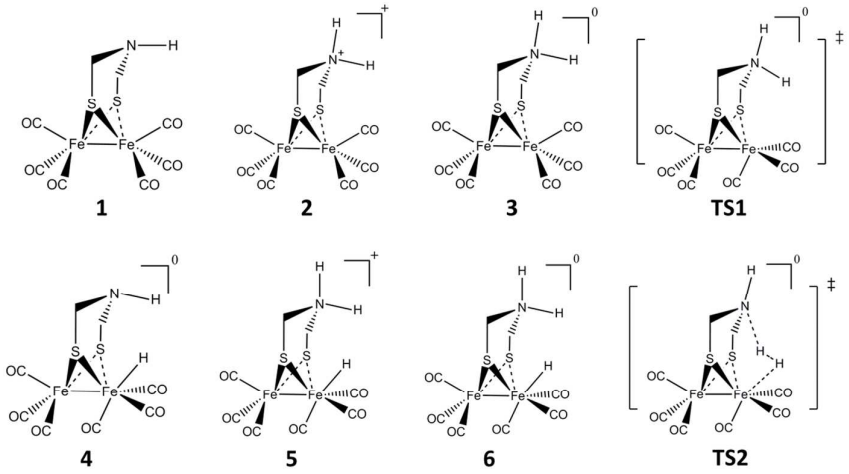

Scheme 2. Structure of the intermediates and transition states involved in the catalysis of electrochemical proton reduction by **1** in the presence of a relatively strong acid in MeCN (pK_a < 10).

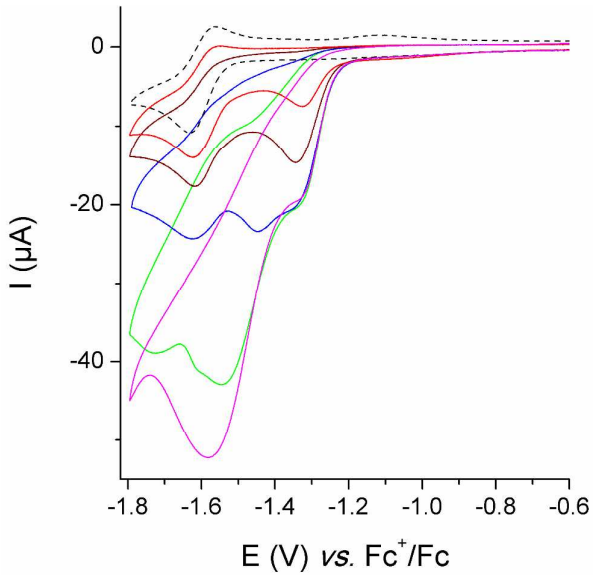

Figure 1. CVs of 0.5 mM **1** in 0.1 M Bu_4NPF_6/MeCN recorded at -10 °C upon successive addition of HOTs (pK_a = 8.7): 0, 1, 2, 4, 8, and 12 mol equiv.

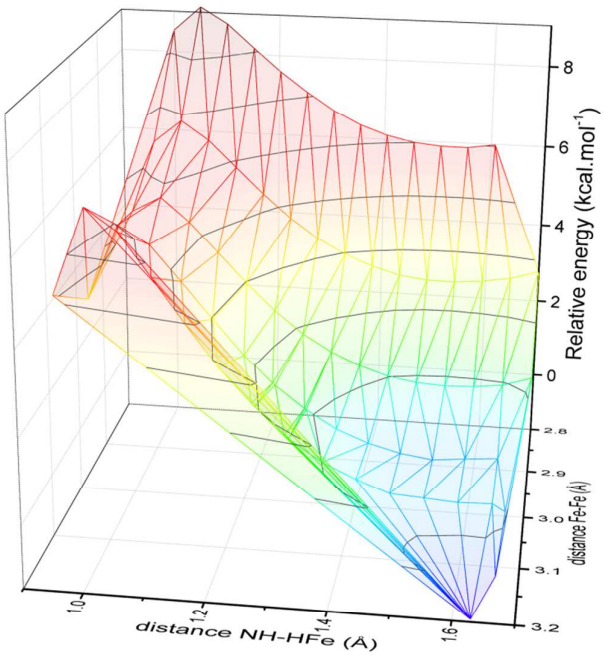

Figure 2. Relaxed potential energy surface scan for the reaction **6** → **1** + H_2 .

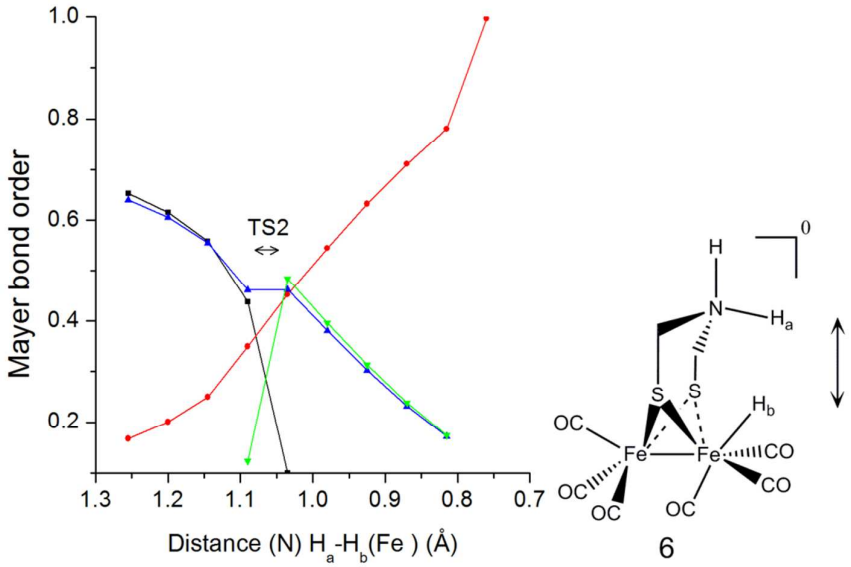

Figure 3. Mayer bond order calculated from the B3LYP/def2-TZVP structures of the N–H_a (black), H_a–H_b (red), Fe–H_b (blue) and Fe–H_a (green) bonds as a function of the H_a–H_b distance in the course of H_2 formation and release from intermediate **6**.

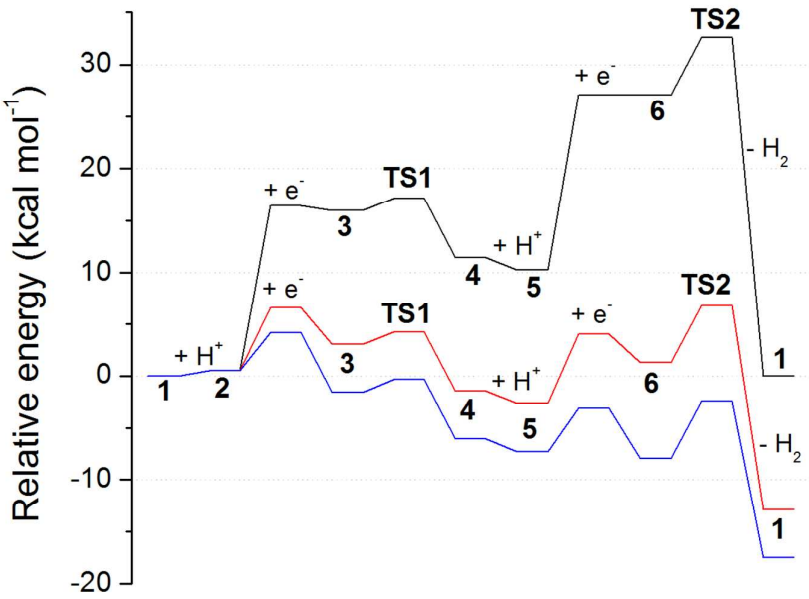

Figure 4. Energetic landscape as a function of the overpotential $\eta = E - E^0_{HA}$ for the catalysis of electrochemical proton reduction by **1** in the presence of HOTs (pK_a = 8.7; E^0_{HA} = –0.54 V vs. $Fc^{+/0}$): η = 0 V (black), –0.56 V (red) and –0.76 V (blue).

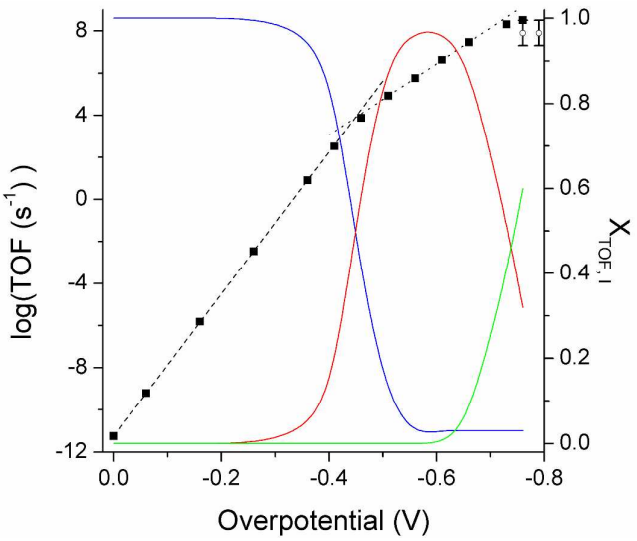

Figure 5. Plot of log TOF as a function of overpotential (black squares) computed from the energetic landscapes established for a range of different values of applied potential *E* (see Table 1). Linear regression (dotted lines) shows two different kinetic regimes characterized by slopes of 30 and 59 mV dec^{-1}, respectively. TOF at high overpotentials calculated from CV measurements is also indicated

(blank circles). Plot of the degree of TOF control $X_{TOF,\ I}$ of some intermediates as a function of overpotential: $X_{TOF,\ 1} + X_{TOF,\ 2}$ (blue trace), $X_{TOF,\ 4} + X_{TOF,\ 5}$ (red trace), and $X_{TOF,\ 6}$ (green trace).

Table 1. Relative free enthalpies of intermediates and corresponding free enthalpies of activation in kcal mol^{-1}, using HOTs as an acid, as used for building the energetic landscapes and calculate the TOF values (for three different values of overpotential given as examples).

η (V)	**1**	**1→2**	**2**	**2 → 3**	**3**	**TS1**	**4**	**4→5**	**5**	**5→6**	**6**	**TS2**	**7**
0	0	4.0	0.5	16.1	16.0	17.2	11.5	15.5	10.3	27.1	27.1	32.6	0
–0.54	0	4.0	0.5	6.4	3.0	4.2	-1.5	2.5	-2.7	4.0	1.3	6.8	-12.9
–0.74	0	4.0	0.5	4.1	-1.6	-0.4	-6.1	-1.6	-7.3	-3.1	-8.0	-25	-17.5

References

1 C. Amatore and A. Jutand, *J. Organomet. Chem.*, 1999, **576**, 254–278.
2 E. Roduner, *Chem Soc Rev*, 2014, **43**, 8226–8239.
3 N. S. Lewis and D. G. Nocera, *Proc. Natl. Acad. Sci.*, 2006, **103**, 15729–15735.
4 D. L. DuBois, *Inorg. Chem.*, 2014, **53**, 3935–3960.
5 C. Costentin, M. Robert and J.-M. Savéant, *Chem. Soc. Rev.*, 2013, **42**, 2423-2436.
6 M. Bourrez, F. Molton, S. Chardon-Noblat and A. Deronzier, *Angew. Chem. Int. Ed.*, 2011, **50**, 9903–9906.
7 J.-D. Compain, M. Bourrez, M. Haukka, A. Deronzier and S. Chardon-Noblat, *Chem. Commun.*, 2014, **50**, 2539-2542.
8 T. A. White, S. Maji and S. Ott, *Dalton Trans.*, 2014, **43**, 15028-15037.
9 B. Kumar, M. Llorente, J. Froehlich, T. Dang, A. Sathrum and C. P. Kubiak, *Annu. Rev. Phys. Chem.*, 2012, **63**, 541–569.
10 J. Schneider, H. Jia, J. T. Muckerman and E. Fujita, *Chem. Soc. Rev.*, 2012, **41**, 2036-2051.
11 J. A. Keith, K. A. Grice, C. P. Kubiak and E. A. Carter, *J. Am. Chem. Soc.*, 2013, **135**, 15823–15829.
12 Y. C. Lam, R. J. Nielsen, H. B. Gray and W. A. Goddard, *ACS Catal.*, 2015, **5**, 2521–2528.
13 X. Sala, S. Maji, R. Bofill, J. García-Antón, L. Escriche and A. Llobet, *Acc. Chem. Res.*, 2014, **47**, 504–516.
14 I. López, M. Z. Ertem, S. Maji, J. Benet-Buchholz, A. Keidel, U. Kuhlmann, P. Hildebrandt, C. J. Cramer, V. S. Batista and A. Llobet, *Angew. Chem.*, 2014, **126**, 209–213.
15 M. D. Kärkäs, O. Verho, E. V. Johnston and B. Åkermark, *Chem. Rev.*, 2014, **114**, 11863–12001.
16 L. Wang, M. Mirmohades, A. Brown, L. Duan, F. Li, Q. Daniel, R. Lomoth, L. Sun and L. Hammarström, *Inorg. Chem.*, 2015, **54**, 2742–2751.
17 V. Fourmond, P.-A. Jacques, M. Fontecave and V. Artero, *Inorg. Chem.*, 2010, **49**, 10338–10347.
18 J. A. S. Roberts and R. M. Bullock, *Inorg. Chem.*, 2013, **52**, 3823–3835.
19 G. A. N. Felton, R. S. Glass, D. L. Lichtenberger and D. H. Evans, *Inorg. Chem.*, 2006, **45**, 9181–9184.
20 S. Chen, M.-H. Ho, R. M. Bullock, D. L. DuBois, M. Dupuis, R. Rousseau and S. Raugei, *ACS Catal.*, 2014, **4**, 229–242.
21 S. Raugei, D. L. DuBois, R. Rousseau, S. Chen, M.-H. Ho, R. M. Bullock and M. Dupuis, *Acc. Chem. Res.*, 2015, **48**, 248–255.
22 C. Costentin, S. Drouet, M. Robert and J.-M. Savéant, *J. Am. Chem. Soc.*, 2012, **134**, 11235–11242.
23 C. Costentin, G. Passard and J.-M. Savéant, *J. Am. Chem. Soc.*, 2015, **137**, 5461–5467.
24 P. Connolly and J. H. Espenson, *Inorg. Chem.*, 1986, **25**, 2684–2688.
25 V. Artero, M. Chavarot-Kerlidou and M. Fontecave, *Angew. Chem. Int. Ed.*, 2011, **50**, 7238–7266.
26 D. Z. Zee, T. Chantarojsiri, J. R. Long and C. J. Chang, *Acc. Chem. Res.*, 2015, **48**, 2027-2038.
27 J. L. Dempsey, B. S. Brunschwig, J. R. Winkler and H. B. Gray, *Acc. Chem. Res.*, 2009, **42**, 1995–2004.

28 N. Queyriaux, R. T. Jane, J. Massin, V. Artero and M. Chavarot-Kerlidou, *Coord. Chem. Rev.*, 2015, doi:10.1016/j.ccr.2015.03.014.
29 M. L. Helm, M. P. Stewart, R. M. Bullock, M. R. DuBois and D. L. DuBois, *Science*, 2011, **333**, 863–866.
30 A. D. Wilson, R. K. Shoemaker, A. Miedaner, J. T. Muckerman, D. L. DuBois and M. R. DuBois, *Proc. Natl. Acad. Sci.*, 2007, **104**, 6951–6956.
31 V. Fourmond, S. Canaguier, B. Golly, M. J. Field, M. Fontecave and V. Artero, *Energy Environ. Sci.*, 2011, **4**, 2417-2427.
32 B. D. McCarthy, C. L. Donley and J. L. Dempsey, *Chem Sci*, 2015, **6**, 2827-2834.
33 F. Gloaguen, J. D. Lawrence and T. B. Rauchfuss, *J. Am. Chem. Soc.*, 2001, **123**, 9476–9477.
34 F. Gloaguen and T. B. Rauchfuss, *Chem. Soc. Rev.*, 2009, **38**, 100–108.
35 S. Tschierlei, S. Ott and R. Lomoth, *Energy Environ. Sci.*, 2011, **4**, 2340-2352.
36 N. Wang, M. Wang, L. Chen and L. Sun, *Dalton Trans.*, 2013, **42**, 12059-12071.
37 T. R. Simmons, G. Berggren, M. Bacchi, M. Fontecave and V. Artero, *Coord. Chem. Rev.*, 2014, **270-271**, 127–150.
38 E. Reisner, *Eur. J. Inorg. Chem.*, 2011, **2011**, 1005–1016.
39 J.-F. Capon, F. Gloaguen, F. Y. Pétillon, P. Schollhammer and J. Talarmin, *Coord. Chem. Rev.*, 2009, **253**, 1476–1494.
40 G. A. N. Felton, C. A. Mebi, B. J. Petro, A. K. Vannucci, D. H. Evans, R. S. Glass and D. L. Lichtenberger, *J. Organomet. Chem.*, 2009, **694**, 2681–2699.
41 D. J. Crouthers, J. A. Denny, R. D. Bethel, D. G. Munoz and M. Y. Darensbourg, *Organometallics*, 2014, **33**, 4747–4755.
42 J. R. McKone, S. C. Marinescu, B. S. Brunschwig, J. R. Winkler and H. B. Gray, *Chem Sci*, 2014, **5**, 865–878.
43 M. Wang, L. Chen and L. Sun, *Energy Environ. Sci.*, 2012, **5**, 6763–6778.
44 V. S. Thoi, Y. Sun, J. R. Long and C. J. Chang, *Chem Soc Rev*, 2013, **42**, 2388–2400.
45 P. D. Tran and J. Barber, *Phys. Chem. Chem. Phys.*, 2012, **14**, 13772-13784.
46 C. H. Lee, D. K. Dogutan and D. G. Nocera, *J. Am. Chem. Soc.*, 2011, **133**, 8775–8777.
47 V. Artero and J.-M. Saveant, *Energy Env. Sci*, 2014, **7**, 3808–3814.
48 S. Lounissi, G. Zampella, J.-F. Capon, L. De Gioia, F. Matoussi, S. Mahfoudhi, F. Y. Pétillon, P. Schollhammer and J. Talarmin, *Chem. - Eur. J.*, 2012, **18**, 11123–11138.
49 C. Liu, J. N. T. Peck, J. A. Wright, C. J. Pickett and M. B. Hall, *Eur. J. Inorg. Chem.*, 2011, **2011**, 1080–1093.
50 C. Riplinger and E. A. Carter, *ACS Catal.*, 2015, **5**, 900–908.
51 Y. C. Lam, R. J. Nielsen, H. B. Gray and W. A. Goddard, *ACS Catal.*, 2015, 2521–2528.
52 S. Kozuch, C. Amatore, A. Jutand and S. Shaik, *Organometallics*, 2005, **24**, 2319–2330.
53 S. Kozuch and S. Shaik, *J. Phys. Chem. A*, 2008, **112**, 6032–6041.
54 S. Kozuch and J. M. L. Martin, *ACS Catal.*, 2012, **2**, 2787–2794.
55 S. Kozuch, *Wiley Interdiscip. Rev. Comput. Mol. Sci.*, 2012, **2**, 795–815.
56 M. Bourrez, R. Steinmetz and F. Gloaguen, *Inorg. Chem.*, 2014, **53**, 10667–10673.
57 J. L. Stanley, T. B. Rauchfuss and S. R. Wilson, *Organometallics*, 2007, **26**, 1907–1911.
58 F. Neese, *Wiley Interdiscip. Rev. Comput. Mol. Sci.*, 2012, **2**, 73–78.
59 J. M. L. Martin and A. Sundermann, *J. Chem. Phys.*, 2001, **114**, 3408-3421.
60 A. Klamt, *Wiley Interdiscip. Rev. Comput. Mol. Sci.*, 2011, **1**, 699–709.
61 R. Izsák, F. Neese and W. Klopper, *J. Chem. Phys.*, 2013, **139**, 094111.

62 I. Mayer, *J. Comput. Chem.*, 2007, **28**, 204–221.
63 M. A. Carvajal, S. Kozuch and S. Shaik, *Organometallics*, 2009, **28**, 3656–3665.
64 A. J. Kresge, *Chem. Soc. Rev.*, 1973, **2**, 475-503.
65 M. Mirmohades, S. Pullen, M. Stein, S. Maji, S. Ott, L. Hammarström and R. Lomoth, *J. Am. Chem. Soc.*, 2014, **136**, 17366–17369.
66 M. T. Huynh, W. Wang, T. B. Rauchfuss and S. Hammes-Schiffer, *Inorg. Chem.*, 2014, **53**, 10301–10311.
67 As indicated by one of the referees, taking a value $\tau = 1$ for the pre-exponential factor is an assumption that is only in part supported by the agreement between the experimental and calculated value of TOF at large overpotentials (Fig. 5). However, such an assumption is not unusual when considering electrochemical reactions. see e.g.: C.P. Andrieux, A. Le Gorande, J.-M. Savéant, *J. Am. Chem. Soc.*, 1992, **114**, 6892-6904 and B. H. Solis and S. Hammes-Schiffer, *Inorg. Chem.*, 2014, **53**, 6427–6443.
68 J. K. Nørskov, J. Rossmeisl, A. Logadottir, L. Lindqvist, J. R. Kitchin, T. Bligaard and H. Jónsson, *J. Phys. Chem. B*, 2004, **108**, 17886–17892.
69 D. R. Weinberg, C. J. Gagliardi, J. F. Hull, C. F. Murphy, C. A. Kent, B. C. Westlake, A. Paul, D. H. Ess, D. G. McCafferty and T. J. Meyer, *Chem. Rev.*, 2012, **112**, 4016–4093.
70 M. Bourrez, R. Steinmetz, S. Ott, F. Gloaguen and L. Hammarström, *Nat. Chem.*, 2015, **7**, 140–145.
71 S. Fletcher, *J. Solid State Electrochem.*, 2009, **13**, 537–549.
72 L. E. Fernandez, S. Horvath and S. Hammes-Schiffer, *J. Phys. Chem. Lett.*, 2013, **4**, 542–546.

A method for the computation of TOF of catalysis of electrochemical reaction as a function of the potential was developed.